Electronic Research Archive

https://www.aimspress.com/journal/era

ERA, 34(2): 938–961.
DOI: 10.3934/era.2026044
Received: 10 December 2025
Revised: 13 January 2026
Accepted: 20 January 2026
Published: 29 January 2026

Research article

Global dynamics of controlled competitive diffusion in heterogeneous environments

Xinyu Wang[1], **Lipu Zhang**[1,2,*], **Xinyuan Jin**[1] **and Yao Tong**[1]

[1] School of Media Engineering, Communication University of Zhejiang, Hangzhou 310018, China

[2] Key Lab of Film and TV Media Technology of Zhejiang Province, Hangzhou 310018, China

* **Correspondence:** Email: zhanglipu@cuz.edu.cn.

Abstract: We establish global well-posedness for a two-species competitive reaction-diffusion system in bounded two-dimensional domains under Neumann boundary conditions. The system incorporates spatially heterogeneous growth continuous over the closed domain and time-dependent bounded asymmetric intervention. A sharp threshold condition relating the target species' promotion strength to its natural decay rate is necessary and sufficient to maintain the carrying-capacity constraint globally in time, with the two species' total density not exceeding 1. Meanwhile, the unit square with both species' densities ranging between 0 and 1 remains positively invariant, regardless of the target species' promotion strength. Solutions are classical and unique, uniformly bounded, and Lipschitz-continuous with respect to initial data. Numerical simulations show that asymptotically applied interventions that satisfy the threshold condition result in a near-complete eradication of the competitor species at full efficiency. The promoted species establishes a heterogeneous spatial distribution shaped by growth heterogeneity. This framework extends classical diffusive Lotka-Volterra models and provides rigorous theoretical support for ecological management and misinformation suppression strategies.

Keywords: reaction-diffusion system; asymptotic intervention; global well-posedness; two-component dynamics; heterogeneous propagation efficiency

1. Introduction

We consider a two-species competitive reaction-diffusion system with spatially heterogeneous growth and time-dependent asymmetric intervention in a bounded C^2 domain $\Omega \subset \mathbb{R}^2$. The

non-negative densities $u(x,t)$ and $v(x,t)$ satisfy the following:

$$\begin{cases} \dfrac{\partial u}{\partial t} = D_1\Delta u + \alpha_1 P(x)u(1-u-v) - \lambda_1 u + \gamma_1 uI(t), \\ \dfrac{\partial v}{\partial t} = D_2\Delta v + \alpha_2 P(x)v(1-u-v) - \lambda_2 v - \gamma_2 vI(t), \end{cases} \tag{1.1}$$

which is subject to homogeneous Neumann boundary conditions and initial data $0 \le u_0, v_0 \in H^1(\Omega)$, with $u_0 + v_0 \le 1$ almost everywhere.

The term $+\gamma_1 uI(t)$ reduces the net mortality of the target species u, while $-\gamma_2 vI(t)$ increases the mortality of the competitor v, thereby modeling asymmetric internal control [1] such as targeted species management or fact-checking in misinformation dynamics. The combination of spatially heterogeneous $P(x)$ and time-dependent $I(t)$ introduces distinct theoretical challenges that are not encountered in classical diffusive Lotka-Volterra systems with constant growth rates and no intervention: (i) the reaction terms become space-time dependent, thus requiring uniform verification of upper/lower solutions over all $x \in \overline{\Omega}$ and $t \ge 0$; (ii) and arbitrary time-varying $I(t)$ precludes a stationary steady-state analysis and demands global-in-time boundedness arguments that account for dynamic control effects. The condition $\gamma_1 \le \lambda_1$ is necessary and sufficient for the carrying-capacity constraint $u(x,t) + v(x,t) \le 1$ to hold for all time, which is a sharp threshold that resolves these challenges by ensuring the reaction vector field points inward on the invariant rectangle $[0,1]^2$. Here, $D_1, D_2 > 0$ are diffusion rates, $\alpha_1, \alpha_2 > 0$ are intrinsic growth rates, and $P \in C(\overline{\Omega})$ with $0 < P_{\min} \le P(x) \le P_{\max}$ describes the spatial heterogeneity, where $P_{\min} = \min_{x\in\overline{\Omega}} P(x)$ denotes the minimum value of the habitat suitability function $P(x)$ over the closed domain $\overline{\Omega}$, $\lambda_1, \lambda_2 > 0$ are natural decay rates, $I \in L^\infty(0,\infty)$ with $0 \le I(t) \le 1$ represents the intervention intensity, and $\gamma_1, \gamma_2 \ge 0$ quantify the intervention strengths. Applications include ecological invasion control [2] and chemical reactor regulation [3]; for the misinformation context, our model builds on mathematical frameworks for structured competing systems under dynamic perturbations [4, 5] to address the suppression of false information.

Classical diffusive Lotka-Volterra models [6–8] often assume constant coefficients or neglect realistic control mechanisms. Limitations of previous studies include oversimplified intervention schemes [9] and inadequate boundary treatments [10]. In particular, the interaction between spatial heterogeneity $P(x)$ and competitive outcomes remains a central challenge [11]. Moreover, recent progress has also explored more complex mechanisms in competitive Lotka-Volterra systems, such as chemorepulsion effects [12] and optimal control problems that incorporate chemo-repulsion [13]. However, these studies typically focus on specific biological features (chemorepulsion) or optimization objectives, and still do not simultaneously address the combination of fully spatially heterogeneous intrinsic growth rates and general time-dependent asymmetric interventions considered in the present work. Recent studies have explored population models with advection effects [14], complex kinetic structures [15], and diffusion-driven global dynamics or long-time behavior [16, 17]. Nevertheless, these works usually relied on assumptions such as equal diffusivities, constant growth rates, or one-dimensional spatial settings, and thus did not capture the combined influence of fully heterogeneous growth and time-dependent asymmetric control. As a result, diffusion-driven spatio-temporal bifurcations in population models remain far from being fully understood. For instance, Li et al. [18] studied the Turing-Hopf bifurcation in a diffusive Leslie-Gower system, complementary to the global invariant analysis pursued here. Additionally, related work [19] has

considered non-smooth or discontinuous intervention structures, which provides a contrast to the continuous framework adopted in the present study. Meanwhile, advances in the numerical scheme design for multi-component nonlinear systems [20, 21] have focused on invariant-preserving and conservative discretization methods for wave and Camassa-Holm systems, thereby providing valuable numerical frameworks to simulate complex dynamical systems but lack a direct integration with heterogeneous competitive diffusion and intervention control scenarios.

To further clarify the novelty and positioning of the present work, we summarize representative reaction-diffusion competition models in Table 1 with respect to the spatial formulation, diffusion structure, control mechanisms, heterogeneity degree, and core analytical focus. This comparison highlights that the combination of fully heterogeneous growth and time-dependent asymmetric interventions, together with the analysis of invariant regions and global well-posedness, distinguishes our study from existing literature.

Table 1. Comparison of representative competitive models in the literature.

Reference	Space	Diffusion	Control	Heterogeneity	Focus
[1]	PDE	Yes	Boundary + Interior	Partial	Controllability to steady states
[2]	PDE	Yes	Spatial allocation	Partial	Optimal spatial invasion control
[5]	PDE	Yes	No	Partial	Steady-state stability
[6]	ODE	–	No	None	Classical LV theory
[7]	PDE	Yes	No	Partial	Heterogeneity effects
[9]	PDE	Yes	No	None	Steady states (fear)
[11]	PDE	Yes	No	Partial	Competitive outcomes
[12]	PDE	Yes	Chemo-repulsion	Partial	Competition + chemorepulsion
[13]	PDE	Yes	Optimal control + chemorepulsion	Partial	Optimal control with chemorepulsion
[14]	PDE	Yes	No	Partial	Threshold & asymptotic profiles
[15]	PDE	Yes	No	Partial	Global boundedness
[16]	PDE	Yes	No	Partial	Global dynamics (advection)
[17]	PDE	Yes	No	Partial	Long-time behavior
[18]	PDE	Yes	No	None	Turing-Hopf bifurcation
This work	PDE	Yes	**Time-dependent asymmetric**	**Full**	**Invariant regions + Global well-posedness**

Notes: Abbreviations: Partial differential equation (PDE); Ordinary differential equation(ODE).

This work develops a framework that simultaneously incorporates spatial heterogeneity $P(x)$, the general time-dependent intervention $I(t)$, and two-dimensional bounded domains with Neumann conditions. The framework allows fully heterogeneous growth to coexist with arbitrary time-varying interventions, identifies the sharp condition $\gamma_1 \leq \lambda_1$ for global preservation of the carrying-capacity constraint $u + v \leq 1$, and establishes the global existence, uniqueness, and classical regularity of solutions with Lipschitz continuous dependence on the initial data. The use of homogeneous Neumann conditions is appropriate for closed habitats [22].

The remainder of this paper is organized as follows: in Section 2, we state the main assumptions and establish the global well-posedness theory, including the sharp threshold $\gamma_1 \leq \lambda_1$ to preserve the carrying-capacity constraint; Section 3 presents finite-difference simulations that verify the theoretical predictions and quantify the long-time suppression effect under asymptotic intervention; and

concluding remarks and potential extensions are given in Section 4.

2. Global well-posedness theory

This section establishes the mathematical foundation for system (1.1), thereby proving the global well-posedness under the critical coefficient constraint $\gamma_1 \leq \lambda_1$. The system is considered for $(x, t) \in \Omega \times (0, \infty)$, with homogeneous Neumann boundary conditions

$$\frac{\partial u}{\partial \mathbf{n}} = 0, \quad \frac{\partial v}{\partial \mathbf{n}} = 0 \quad \text{on } \partial\Omega \times (0, \infty), \tag{2.1}$$

and initial conditions

$$u_0, v_0 \geq 0 \text{ and } u_0 + v_0 \leq 1, \tag{2.2}$$

almost everywhere, where $u_0, v_0 \in H^1(\Omega)$, and $\mathbf{n}$ is the outward unit normal.

2.1. Some lemmas

The reaction terms

$$R_1(u, v, x, t) = \alpha_1 P(x)u(1 - u - v) - \lambda_1 u + \gamma_1 u I(t)$$

and

$$R_2(u, v, x, t) = \alpha_2 P(x)v(1 - u - v) - \lambda_2 v - \gamma_2 v I(t)$$

exhibit type-K quasimonotonicity [23], since the off-diagonal Jacobian entries

$$\frac{\partial R_1}{\partial v} = -\alpha_1 P(x)u \leq 0 \quad \text{and} \quad \frac{\partial R_2}{\partial u} = -\alpha_2 P(x)v \leq 0,$$

on $[0, 1]^2 \times \overline{\Omega}$ (the intervention terms are diagonal and thus preserve the property). This structure induces an order-preserving flow, thereby enabling the use of comparison principles [24] and invariant-region techniques [25] in the subsequent well-posedness analysis; moveover, for general results on reaction-diffusion systems with Neumann boundary conditions, see [26].

Lemma 1 (lower solution and non-negativity)**.** *The constant pair* $(\underline{u}, \underline{v}) \equiv (0, 0)$ *is a lower solution for the systems* (1.1)–(2.2)*. Consequently, any solution satisfies* $u(x, t) \geq 0$ *and* $v(x, t) \geq 0$ *almost everywhere in* $\Omega \times (0, T_{\max})$.

Proof. Let $T_{\max}$ denote the maximal existence time of the local classical solution to systems (1.1)–(2.2), which is guaranteed by the local existence and uniqueness theorem for semilinear parabolic systems [27] due to the Lipschitz continuity of the reaction terms R_1 and R_2. $T_{\max}$ is the largest positive real number such that the solution remains bounded on $[0, T_{\max})$; its finiteness implies solution blow-up, while $T_{\max} = \infty$ corresponds to the global existence. Set $u^- = \max\{0, -u\}$. For any $t \in (0, T_{\max})$, the function $u^-(t)$ belongs to $H^1(\Omega)$ and satisfies $\partial_n u^- = 0$ on $\partial\Omega$. Testing the first equation with u^- gives the following:

$$\frac{1}{2}\frac{\mathrm{d}}{\mathrm{d}t}\int_\Omega (u^-)^2\,dx + D_1 \int_\Omega |\nabla u^-|^2\,dx = -\int_\Omega R_1(u, v, x, t)\,u^-\,dx.$$

When $u < 0$, we have $u^- = -u > 0$ and

$$R_1(u, v, x, t) = u\big[\alpha_1 P(x)(1 - u - v) - \lambda_1 + \gamma_1 I(t)\big] =: u\, B(x, t),$$

with $|B(x, t)| \le C_0$ by the boundedness of the local classical solution on $[0, T)$ for $T < T_{\max}$ (guaranteed by the definition of $T_{\max}$). Hence,

$$-\int_\Omega R_1\, u^-\, dx = \int_\Omega B(x, t)\,(u^-)^2\, dx \le C_0 \int_\Omega (u^-)^2\, dx.$$

Dropping the nonnegative diffusion term, we obtain the following:

$$\frac{\mathrm{d}}{\mathrm{d}t}\int_\Omega (u^-)^2\, dx \le 2C_0 \int_\Omega (u^-)^2\, dx.$$

Since $u^-(0) = 0$, Grönwall's lemma [28] yields $u^-(t) \equiv 0$ (i.e., $u(x, t) \ge 0$). When applied to v, the same argument gives $v(x, t) \ge 0$. □

Lemma 2 (Upper Solution Under Coefficient Constraint)**.** *Under $\gamma_1 \le \lambda_1$, the constant pair $(\overline{u}, \overline{v}) \equiv (1, 1)$ is an upper solution for the system.*

Proof. Set $(\overline{u}, \overline{v}) \equiv (1, 1)$. Time derivatives and Laplacians vanish. For the reaction terms, we have $1 - \overline{u} - \overline{v} = -1$, so

$$\begin{aligned} R_1(\overline{u}, \overline{v}) &= \alpha_1 P(x) \cdot 1 \cdot (-1) - \lambda_1 + \gamma_1 I(t) = -\alpha_1 P(x) - (\lambda_1 - \gamma_1 I(t)) \\ &\le -\alpha_1 P_{\min} - (\lambda_1 - \gamma_1) \le 0, \end{aligned}$$

where we use $P(x) \ge P_{\min} > 0$, $I(t) \le 1$ and the assumption $\gamma_1 \le \lambda_1$. Similarly,

$$R_2(\overline{u}, \overline{v}) = \alpha_2 P(x) \cdot 1 \cdot (-1) - \lambda_2 - \gamma_2 I(t) \le -\alpha_2 P_{\min} < 0.$$

Homogeneous Neumann boundary conditions give $\partial_n \overline{u} = \partial_n \overline{v} = 0 \ge 0$. Finally, the initial constraint $u_0 + v_0 \le 1$ together with non-negativity of u_0, v_0 implies $u_0 \le 1$, $v_0 \le 1$ a.e. in Ω. Hence, $(1, 1)$ is an upper solution. □

Lemma 3 (Invariant region and sharp threshold)**.** *The rectangle $\mathcal{R} = [0, 1]^2$ is positively invariant for systems* (1.1)–(2.2) *for all $\gamma_1, \gamma_2 \ge 0$. Moreover, the carrying-capacity constraint $u(x, t) + v(x, t) \le 1$ is preserved for all $t \ge 0$ if and only if $\gamma_1 \le \lambda_1$, which is a sharp and biologically natural threshold.*

Proof. First, we establish the positive invariance of $\mathcal{R} = [0, 1]^2$ under the condition $\gamma_1 \le \lambda_1$ (we derive the key threshold later).

Consider the constant functions $(\overline{u}, \overline{v}) = (1, 1)$; direct calculation yields

$$R_1(1, 1) = -\alpha_1 P(x) - \lambda_1 + \gamma_1 I(t) \le -\alpha_1 P_{\min} - (\lambda_1 - \gamma_1) \le 0$$

and

$$R_2(1, 1) = -\alpha_2 P(x) - \lambda_2 - \gamma_2 I(t) \le -\alpha_2 P_{\min} < 0,$$

with $\partial_{\mathbf{n}} 1 = 0$ on $\partial\Omega$. On the faces $u = 0$ and $v = 0$, we have $R_1(0, v) = 0$ and $R_2(u, 0) = 0$, respectively. Since the system is competitive (i.e., $\partial_v R_1 \le 0$ and $\partial_u R_2 \le 0$), the standard invariant

rectangle theorem for parabolic systems with Neumann boundary conditions implies that $\mathcal{R} = [0, 1]^2$ is positively invariant for $\gamma_1 \leq \lambda_1$ and any $\gamma_2 \geq 0$.

Next, we prove the equivalence between $\gamma_1 \leq \lambda_1$ and the preservation of the carrying-capacity constraint $u + v \leq 1$ for all $t \geq 0$. For the sufficiency, assume $\gamma_1 \leq \lambda_1$; on the face $u = 1$ with $0 \leq v \leq 1$, we obtain

$$R_1(1, v) = -\alpha_1 P(x)v - \lambda_1 + \gamma_1 I(t) \leq -\alpha_1 P_{\min} v - (\lambda_1 - \gamma_1) \leq 0,$$

due to $I(t) \leq 1$. For the remaining three faces, the verification is analogous to that in Lemmas 1 and 2, thereby ensuring that the reaction vector field points inward or is tangent on $\partial\mathcal{R}$. This invariance of $\mathcal{R}$ further guarantees $u(x, t) + v(x, t) \leq 1$ for all $t \geq 0$.

For necessity, suppose $\gamma_1 > \lambda_1$ and denote $\delta = \gamma_1 - \lambda_1 > 0$. We start with the constant $I(t) \equiv 1$ case and then extend to the non-constant $I(t)$. For the constant $I(t) \equiv 1$, take the constant initial data $u_0 = 1 - \eta$ (with $0 < \eta < 1$) and $v_0 = 0$; it follows that $v(x, t) = 0$ for all $t \geq 0$, and u satisfies the following scalar logistic equation:

$$\partial_t u = D_1 \Delta u + \alpha_1 P(x)u(1 - u) + \delta u.$$

The constant $\overline{u} = 1$ is no longer an upper solution because $R_1(1, 0) = \delta > 0$, and as shown in [7], all positive solutions of this equation converge to a unique positive steady state $u^* > 1$. This implies

$$u(x, t) + v(x, t) = u(x, t) > 1,$$

for large t, which violates the carrying-capacity constraint (while still satisfying $0 \leq u \leq M$ and $0 \leq v \leq 1$ for some $M > 1$).

For the non-constant $I(t)$, the analysis relies on the maximum intensity of $I(t)$. If $\sup_{t\geq 0} I(t) > \lambda_1/\gamma_1$, there exists a time interval $[t_1, t_2]$ such that $I(t) \geq I_0 > \lambda_1/\gamma_1$ for all $t \in [t_1, t_2]$. Choosing the initial data at $t = t_1$ as $u(t_1) = 1 - \eta$ (with $0 < \eta < 1$) and $v(t_1) = 0$, the u-equation on $[t_1, t_2]$ takes the following form:

$$\partial_t u = D_1 \Delta u + \alpha_1 P(x)u(1 - u) + (\gamma_1 I(t) - \lambda_1)u.$$

Since $\gamma_1 I(t) - \lambda_1 \geq \gamma_1 I_0 - \lambda_1 > 0$, the extra positive growth term drives $u(x, t)$ to exceed 1 within $[t_1, t_2]$, which violates $u + v \leq 1$. If

$$\sup_{t\geq 0} I(t) \leq \lambda_1/\gamma_1,$$

then

$$\gamma_1 I(t) - \lambda_1 \leq 0,$$

for all $t \geq 0$, and the carrying-capacity constraint is trivially preserved. However, this scenario corresponds to ineffective intervention for promoting u, as the promotion term cannot offset the natural decay of u, so $\gamma_1 \leq \lambda_1$ is necessary to preserve the constraint in all effective intervention regimes (where $I(t)$ is large enough to meaningfully promote u).

Finally, we confirm the sharpness of $\gamma_1 \leq \lambda_1$. The above analysis for both constant and non-constant $I(t)$ shows that when $\gamma_1 > \lambda_1$, even intermittent high-intensity intervention (effective regime) will eventually violate $u + v \leq 1$, while when $\gamma_1 = \lambda_1$, the constraint is preserved by the sufficiency result. Thus, $\gamma_1 \leq \lambda_1$ is sharp to preserve $u + v \leq 1$ globally in time, regardless of $I(t)$ in the effective intervention regimes.

In summary, for all applications where the total density must respect a strict carrying capacity $u + v \leq 1$ (e.g., classical competitive Lotka-Volterra models or normalized information densities), the condition $\gamma_1 \leq \lambda_1$ is necessary and sufficient. □

2.2. Regularity of classical solutions

In this subsection, we justify the regularity of solutions and show that the weak solutions obtained above are in fact classical.

Let $u_0, v_0 \in H^1(\Omega)$ with $0 \leq u_0, v_0 \leq 1$ almost everywhere in Ω. Since the reaction terms R_1 and R_2 are locally Lipschitz and the invariant region $\mathcal{R} = [0, 1]^2$ is positively invariant, the systems (1.1)–(2.2) admits a unique global weak solution as follows:

$$(u, v) \in L^\infty(0, T; H^1(\Omega)) \cap H^1(0, T; H^{-1}(\Omega));$$

for instance, see Lunardi [27].

Moreover, due to the diagonal diffusion structure, boundedness of solutions, and Lipschitz continuity of the reaction terms on $\mathcal{R}$, the De Giorgi-Nash-Moser theory for parabolic equations with Neumann boundary conditions implies that

$$u, v \in C^{\alpha,\alpha/2}(\overline{\Omega} \times [0, T]),$$

for some $0 < \alpha < 1$; see Lieberman [29].

Since R_1 and R_2 are Lipschitz continuous on $\mathcal{R}$ and $(u, v) \in C^{\alpha,\alpha/2}$, it follows that the source terms $R_1(u, v)$ and $R_2(u, v)$ also belong to $C^{\alpha,\alpha/2}(\overline{\Omega}\times[0, T])$. Consequently, each component $w \in \{u, v\}$ satisfies a linear parabolic equation with a constant diffusion coefficient and Hölder continuous right-hand side as follows:

$$\partial_t w - D_w \Delta w = R_w(u, v).$$

By the parabolic Schauder estimates for equations with homogeneous Neumann boundary conditions (see Lieberman [29]), we obtain the higher regularity as follows:

$$w \in C^{2+\alpha,\, 1+\alpha/2}(\overline{\Omega} \times [0, T]).$$

In particular, the weak solutions constructed above are classical solutions of systems (1.1)–(2.2).

2.3. Continuous dependence on initial data

The solutions to systems (1.1)–(2.2) depend Lipschitz continuously on the initial data (u_0, v_0). Let (u_1, v_1) and (u_2, v_2) be two solutions that corresponds to the initial data (u_{01}, v_{01}) and (u_{02}, v_{02}), respectively. Define the differences as follows:

$$w = u_1 - u_2, \qquad z = v_1 - v_2.$$

Subtracting the two systems yields the following:

$$\partial_t w - D_1 \Delta w = R_1(u_1, v_1) - R_1(u_2, v_2), \qquad \partial_t z - D_2 \Delta z = R_2(u_1, v_1) - R_2(u_2, v_2).$$

Multiplying the first equation by w and the second by z, integrating over Ω, and using the Lipschitz continuity of the reaction terms together with the Gronwall inequality, we obtain the following:

$$\|w(\cdot, t)\|_{L^2(\Omega)} + \|z(\cdot, t)\|_{L^2(\Omega)} \leq L\left(\|u_{01} - u_{02}\|_{L^2(\Omega)} + \|v_{01} - v_{02}\|_{L^2(\Omega)}\right),$$

where $L > 0$ denotes a Lipschitz constant depending on the reaction parameters and the time horizon T.

2.3.1. Critical note on the Lipschitz constant

The constant L admits the following estimate:

$$L = C\exp(CT\max\{|\alpha_1|,|\alpha_2|,|\lambda_1|,|\lambda_2|,|\gamma_1|,|\gamma_2|\}),$$

where $C > 0$ is independent of the system parameters, and $T > 0$ denotes the time horizon. This estimate shows that L exponentially grows with respect to both the magnitude of the parameters $(\alpha_i, \lambda_i, \gamma_i)$ and the time interval length T, and may blow up as the parameters become arbitrarily large or as $T \to \infty$. For practical applications that involves finite time horizons and bounded parameters (for instance, physically meaningful growth rates α_i and intervention intensities γ_i), the constant L remains finite, thereby ensuring stable dependence on the initial data. In contrast, for unbounded parameters or infinite time horizons, this stability is not uniform: small perturbations in the initial data may lead to large deviations in the solutions, which is a natural and well-known feature of nonlinear competitive reaction-diffusion systems.

2.4. Main theory

Throughout this section, we work under the standing assumptions introduced in Section 1, namely that $\Omega \subset \mathbb{R}^2$ is a bounded C^2 domain, $P \in C(\overline{\Omega})$ satisfies $0 < P_{\min} \le P(x) \le P_{\max}$, $I \in L^\infty(0,\infty)$ with $0 \le I(t) \le 1$, and all model parameters are nonnegative.

While our analysis uses standard tools from the semilinear parabolic theory (e.g., invariant-region principles, comparison arguments [27,30]), its novelty lies in the tailoring of these techniques to handle the dual heterogeneities of $P(x)$ and $I(t)$-a combination that has not been systematically addressed in classical competitive reaction-diffusion frameworks.

Theorem 1 (Global well-posedness)**.** *Assume $\gamma_1 \le \lambda_1$ and $u_0, v_0 \in L^\infty(\Omega)$ with $0 \le u_0, v_0$, $u_0 + v_0 \le 1$ a.e. in Ω. Then, the system admits a unique global classical solution*

$$(u,v) \in C([0,\infty); H^1(\Omega))^2 \cap L^\infty(0,\infty; L^\infty(\Omega))^2 \cap L^\infty(0,\infty; H^2(\Omega))^2,$$

that satisfies

$$0 \le u(x,t),\ v(x,t) \le 1, \qquad u(x,t) + v(x,t) \le 1 \quad \text{a.e. in } \Omega \times [0,\infty).$$

Moreover, the solution map $(u_0, v_0) \mapsto (u(t), v(t))$ is Lipschitz continuous from $L^2(\Omega)^2$ to itself on any bounded time interval.

Additionally, if $u_0, v_0 \in C^{2+\alpha}(\overline{\Omega})$ for some $0 < \alpha < 1$, with compatible homogeneous Neumann boundary conditions $\partial_{\mathbf{n}} u_0 = \partial_{\mathbf{n}} v_0 = 0$ on $\partial\Omega$ (consistent with the PDE boundary conditions), then the solution enjoys higher Hölder regularity as follows:

$$(u,v) \in C^{2+\beta,1+\beta/2}(\overline{\Omega} \times [0,\infty))^2 \quad \text{for some } 0 < \beta \le \alpha.$$

Proof. First, by Lemma 1, any solution satisfies $u(x,t) \ge 0$ and $v(x,t) \ge 0$ for $t \in [0, T_{\max})$. To establish the upper bounds, consider the reaction vector $R = (R_1, R_2)$ on the boundary faces of the rectangle $\mathcal{R} = [0,1]^2$. On the face $u = 0$ with $v \in [0,1]$, $R_1(0,v) = 0 \ge 0$. On the face $v = 0$ with $u \in [0,1]$, $R_2(u,0) = 0 \ge 0$. On the face $u = 1$ with $v \in [0,1]$,

$$R_1(1,v) = -\alpha_1 P(x) v - \lambda_1 + \gamma_1 I(t) \le -\alpha_1 P_{\min} v - (\lambda_1 - \gamma_1) \le 0,$$

where we use $P_{\min} > 0$ and the assumption $\gamma_1 \le \lambda_1$. Similarly, on the face $v = 1$ with $u \in [0,1]$, $R_2(u,1) = -\alpha_2 P(x)u - \lambda_2 - \gamma_2 I(t) \le 0$. Thus, the reaction vector points inward or is tangent to the boundary on every face of $\mathcal{R}$.

Since $\partial_v R_1 = -\alpha_1 P(x)u \le 0$ and $\partial_u R_2 = -\alpha_2 P(x)v \le 0$, the system is competitive (monotone in the sense of Hirsch for parabolic systems). By the invariant rectangle principle for parabolic systems with homogeneous Neumann boundary conditions, $\mathcal{R} = [0,1]^2$ is positively invariant. Therefore,

$$0 \le u(x,t),\ v(x,t) \le 1, \qquad u(x,t) + v(x,t) \le 1 \quad \forall t \ge 0.$$

Next, rewrite the system in vector form as follows:

$$U_t = \mathcal{D}\Delta U + R(U), \qquad U = (u,v)^\top, \qquad \mathcal{D} = \mathrm{diag}(D_1, D_2).$$

On the compact invariant set $\mathcal{R} = [0,1]^2$, the nonlinearity R is C^1 and globally Lipschitz (with Lipschitz constant depending on $\alpha_1, \alpha_2, P_{\max}, \lambda_1, \lambda_2, \gamma_1, \gamma_2$). The standard local existence theory for semilinear parabolic systems [27] yields a unique maximal classical solution $U \in C([0, T_{\max}); H^1(\Omega))^2$. Since $U(t)$ remains in $\mathcal{R}$ for all $t \in [0, T_{\max})$, we have the uniform bound $\|U\|_{L^\infty(\Omega \times [0, T_{\max}))} \le 1$.

To rule out blow-up in finite time, multiply the equation for u by $-\Delta u$ and integrate over Ω, thereby using the homogeneous Neumann boundary condition $\partial_{\mathbf{n}} u = 0$ (which implies $\int_\Omega \nabla u \cdot \nabla(\Delta u) dx = -\int_\Omega |\Delta u|^2 dx$):

$$\frac{1}{2}\frac{d}{dt}\|\nabla u\|_{L^2}^2 + D_1 \|\Delta u\|_{L^2}^2 = \int_\Omega R_1(u,v)\Delta u \, dx.$$

Taking absolute values on the right-hand side and using the uniform bound $|R_1(u,v)| \le C_1$ (where $C_1 = \alpha_1 P_{\max} + \lambda_1 + \gamma_1$), we obtain the following:

$$\left| \int_\Omega R_1(u,v)\Delta u \, dx \right| \le C_1 \|\Delta u\|_{L^2} |\Omega|^{1/2}.$$

By Young's inequality ($ab \le \frac{a^2}{2\epsilon} + \frac{\epsilon b^2}{2}$ with $\epsilon = D_1/(2C_1|\Omega|^{1/2})$),

$$C_1 |\Omega|^{1/2} \|\Delta u\|_{L^2} \le \frac{D_1}{2}\|\Delta u\|_{L^2}^2 + \frac{C_1^2 |\Omega|}{D_1}.$$

Substituting back gives the follows:

$$\frac{d}{dt}\|\nabla u\|_{L^2}^2 + D_1 \|\Delta u\|_{L^2}^2 \le \frac{2C_1^2 |\Omega|}{D_1}.$$

Integrating over $[0,t]$ and applying Gronwall's inequality (the right-hand side is a constant), we find that $\|\nabla u(t)\|_{L^2}^2$ and $\|\Delta u(t)\|_{L^2}^2$ remain bounded on $[0, T_{\max})$. The same argument applies to v, so $T_{\max} = \infty$ and $u, v \in L^\infty(0, \infty; H^2(\Omega))$.

To obtain a higher Hölder regularity, we assume the initial data satisfy $u_0, v_0 \in C^{2+\alpha}(\overline{\Omega})$ (for some $0 < \alpha < 1$) with compatible homogeneous Neumann boundary conditions (i.e., $\partial_{\mathbf{n}} u_0 = \partial_{\mathbf{n}} v_0 = 0$ on $\partial\Omega$, consistent with the PDE boundary conditions). This is a standard regularity requirement to close the bootstrap argument in the parabolic Schauder theory on bounded C^2 domains.

By the Sobolev embedding theorem in 2D ($H^2(\Omega) \hookrightarrow C^{0,\gamma}(\overline{\Omega})$ for any $\gamma < 1$) and the Gagliardo-Nirenberg interpolation inequality, the uniform H^2 bound implies $u, v \in C^{0,\gamma}(\overline{\Omega})$ for all $t \ge 0$. Since

$I(t) \in L^\infty(0,\infty)$ and $P(x) \in C(\overline{\Omega})$, the reaction terms $R_1(u,v), R_2(u,v)$ inherit the Hölder continuity in space and time with exponent $\alpha' = \min\{\alpha, \gamma\}$. Thus, each component $w \in \{u, v\}$ satisfies a linear parabolic equation:

$$\partial_t w - D_w \Delta w = f(x,t), \qquad f = R_w(u,v) \in C^{\alpha',\alpha'/2}(\overline{\Omega} \times [0,T])$$

for any finite $T > 0$.

Applying the parabolic Schauder estimates for homogeneous Neumann boundary conditions [29], we obtain the following a priori estimate:

$$\|w\|_{C^{2+\alpha',1+\alpha'/2}(\overline{\Omega}\times[0,T])} \le C\left(\|f\|_{C^{\alpha',\alpha'/2}(\overline{\Omega}\times[0,T])} + \|w_0\|_{C^{2+\alpha'}(\overline{\Omega})}\right),$$

where C is a constant independent of T. This implies that the spatial gradients ∇w are Hölder continuous with exponent α', so $w \in C^{1+\alpha,\alpha/2}(\overline{\Omega} \times [0,T])$ (setting $\alpha = \alpha'$). The high regularity of the initial data ensures compatibility at $t = 0$, thus completing the bootstrap argument for Hölder regularity.

Finally, to prove the Lipschitz continuous dependence on the initial data, let $U_1 = (u_1, v_1)$ and $U_2 = (u_2, v_2)$ be two solutions with initial data $U_{01} = (u_{01}, v_{01})$ and $U_{02} = (u_{02}, v_{02})$. Set $W = U_1 - U_2$; then, W satisfies the following:

$$W_t = \mathcal{D}\Delta W + R(U_1) - R(U_2).$$

Taking the L^2 inner product with W and integrating over Ω yields the following:

$$\frac{1}{2}\frac{d}{dt}\|W\|_{L^2}^2 = \int_\Omega W \cdot (R(U_1) - R(U_2))\, dx.$$

Since R is globally Lipschitz on $\mathcal{R}$ with the Lipschitz constant L, we have $|R(U_1) - R(U_2)| \le L|U_1 - U_2|$. By the Cauchy-Schwarz inequality,

$$\int_\Omega W \cdot (R(U_1) - R(U_2))\, dx \le L\|W\|_{L^2}^2.$$

Gronwall's inequality yields the following:

$$\|W(t)\|_{L^2} \le e^{Lt}\|W(0)\|_{L^2},$$

which proves the Lipschitz continuous dependence of the solution map on initial data in $L^2(\Omega)^2$ for any bounded time interval $[0,T]$. The uniqueness of the maximal solution directly follows from this estimate, thus completing the proof. □

In particular, Theorem 1 shows that under the natural intervention constraint $\gamma_1 \le \lambda_1$, the system remains globally well behaved: solutions exist for all time, stay uniformly bounded, and respect the carrying-capacity constraint despite the spatial heterogeneity and time-dependent intervention.

This global well-posedness result lays a foundation to understands the long-time dynamics of the system. For the practically relevant scenario of asymptotic intervention (i.e., the intervention intensity $I(t)$ converges to a constant I_∞ as $t \to \infty$), the uniform boundedness and regularity of solutions guaranteed by Theorem 1 imply that solutions will converge to ecologically meaningful steady states. Notably, a targeted intervention on the competitor species v (via the parameter γ_2) can effectively suppress v to extinction in the steady state, which is a key outcome for ecological management. Additionally, this suppression steady state is stable against small perturbations, thus ensuring the reliability of intervention effects in practical applications.

3. Numerical simulation

Numerical simulations were performed to investigate the dynamics of target and competing species under asymptotic intervention and heterogeneous habitat suitability. Based on the reaction-diffusion system (1.1), the simulations validate that asymptotic intervention effectively suppresses the invasive species while maintaining the carrying-capacity constraint $u + v \leq 1$, and confirm the theoretical predictions of global well-posedness and convergence to a heterogeneous steady state.

For the spatial heterogeneity function $P(x)$, we set $P_{\min} = 0.6$ and $P_{\max} = 1.0$ (Table 2). Theoretically, $P_{\min}$ is a general positive constant determined by the specific form of $P(x)$, while the value 0.6 here is a typical setting to simulate practical habitat heterogeneity scenarios. The spatial and temporal discretizations listed in Table 2 were chosen in accordance with the diffusion coefficients to ensure numerical stability, and additional refinement tests confirmed that the reported results were qualitatively robust.

Table 2. Numerical simulation parameters.

Parameter	Symbol & value	Description
Diffusion	$D_1 = D_2 = 0.1$	Coefficients for u, v
Growth rates	$\alpha_1 = 2.0$, $\alpha_2 = 1.5$	For u, v
Decay rates	$\lambda_1 = 0.5$, $\lambda_2 = 0.3$	For u, v
Intervention	$\gamma_1 = 0.4$, $\gamma_2 = 0.2$	Coefficients for u, v
Asymptotic bound	$I_\infty = 0.8$	Limit of $I(t)$
Heterogeneity	$P_{\min} = 0.6$, $P_{\max} = 1.0$	Propagation efficiency bounds
Spatial discretization	$n_x \times n_y = 50 \times 50$	Grid points
Temporal discretization	$T = 50.0$, $\Delta t = 0.01$	Time, step

1) Error convergence: Monitor H^1 error

$$\|u - u^*\|_{H^1} = \|\nabla(u - u^*)\|_2 + \|u - u^*\|_2$$

and L^∞ error

$$\|u - u^*\|_{L^\infty} = \max |u - u^*|,$$

and similarly for v. A decreasing trend of $\|u - u^*\|$ and $\|v - v^*\|$ over t verifies convergence to the steady state (u^*, v^*), as predicted by Theorem 1.

2) Temporal trend: Here, $\langle u \rangle$ and $\langle v \rangle$ denote the spatial averages over Ω, defined by the following:

$$\langle u \rangle = \frac{1}{|\Omega|} \int_\Omega u \, \mathrm{d}x \, \mathrm{d}y, \qquad \langle v \rangle = \frac{1}{|\Omega|} \int_\Omega v \, \mathrm{d}x \, \mathrm{d}y.$$

We record $\langle u \rangle$, $\langle v \rangle$, together with $I(t) = I_\infty(1 - e^{-0.1t})$—a concrete asymptotic example within the general $I \in L^\infty(0, \infty)$.

3) Spatial distribution: Visualize the final $u(x, y)$ and $v(x, y)$. Consistency between $u(x, y)$, heterogeneous $P(x)$, and $v(x, y) \approx 0$ (uniformly distributed) confirm the spatial characteristics of propagation and suppression under heterogeneity.

4) Quantitative indicators: Calculate the Intervention efficiency ($\eta = \frac{v_0 - v^*}{v_0}$ (v_0 is initial $\langle v \rangle$)) and Convergence rate (slope of $\log(\|u - u^*\|)$ vs. $\log(t)$ (via polyfit)) to quantitatively support theoretical conclusions on the dynamics and well-posedness.

3.1. Numerical method

To ensure the reproducibility and reliability of numerical results, we detail the numerical algorithm, its stability properties, and validation tests as follows.

1) Spatial and temporal discretization: All numerical simulations adopt a second-order accurate 5-point central difference scheme for spatial discretization, with a uniform 50×50 grid (grid spacing $\Delta x = \Delta y \approx 0.0204$) applied to the 2D computational domain $\Omega = [0, 1] \times [0, 1]$. The Laplacian operator Δ is approximated via this 5-point scheme, which is implemented using a sparse matrix to improve the computational efficiency. For the time integration, a Crank-Nicolson semi-implicit scheme (second-order temporally accurate) is employed, where the linear diffusion term ($D_1\Delta u, D_2\Delta v$) is implicitly treated to guarantee unconditional numerical stability, and the nonlinear reaction terms (e.g., $\alpha_1 P(x)u(1 - u - v)$) and intervention terms (e.g., $\gamma_1 uI(t)$) are explicitly treated to simplify the solution of nonlinear systems. The time step is set to $\Delta t = 0.01$ with a total simulation time $T = 50.0$, which satisfies the Courant-Friedrichs-Lewy (CFL) condition for the explicit treatment of reaction terms and balances the computational efficiency and accuracy. Homogeneous Neumann boundary conditions are enforced by symmetric extension of grid points at domain boundaries, thus ensuring no-flux conditions for both u and v.

2) Discrete invariant preservation: To maintain consistency with the theoretical invariant region $0 \leq u, v \leq 1$ and $u + v \leq 1$ (Theorem 1), a two-step post-processing strategy is applied at every time step: (i) clipping u and v to the interval $[0, 1]$ to ensure non-negativity and upper bounds; and (ii) normalizing u and v at grid points where $u + v > 1$ via $u = u/(u + v)$ and $v = v/(u + v)$ to strictly satisfy $u + v = 1$. Numerical validation confirms that this strategy ensures global adherence to the invariant region, with less than 0.3% of grid points requiring normalization across the entire simulation.

3) Validation tests: Two key tests are performed to verify the reliability of the numerical method: (a) Discrete invariant verification: At each time step, we explicitly check that $0 \leq u, v \leq 1$ and $u + v \leq 1$ hold globally, with no persistent violations observed after post-processing. (b) Mesh refinement convergence test: For the representative asymptotic intervention case, grid resolution is refined from 25×25 (coarse) to 100×100 (fine), with the corresponding time steps adjusted to $\Delta t = 0.02, 0.01, 0.005$ (to maintain consistency). The L^∞ error between numerical and theoretical steady states ($u^* = 0.8875, v^* = 0$) monotonically decreases with grid refinement (Table 3), thereby confirming that the numerical solution converges to the theoretical result as $\Delta x, \Delta t \to 0$.

Table 3. Convergence results under mesh refinement (asymptotic intervention, heterogeneous habitat).

Grid resolution	$\Delta x/\Delta y$	Δt	$E_\infty(u)$	$E_\infty(v)$
25×25 (coarse)	0.0417	0.02	0.0215	0.0189
50×50 (medium)	0.0204	0.01	0.0128	0.000004
100×100 (fine)	0.0101	0.005	0.0031	0.000001

Note: $E_\infty = \max|u_{\text{num}} - u^*|$ (or $\max|v_{\text{num}} - v^*|$), with theoretical steady states $u^* = 0.8875$, $v^* = 0$. The medium grid results match our core simulation outputs (final steady-state deviation: $E_\infty(u) = 0.012837$, $E_\infty(v) = 0.000004$).

3.2. *Simulation results*

Under the scenario of asymptotic intervention and heterogeneous habitat suitability ($P(x)$ varies spatially), numerical simulations were conducted to investigate the evolution of protected native (u) and invasive (v) species. As shown in Figure 1, the error curves (top-left) demonstrate global convergence to the steady state, where the native species u approaches $u^* = 0.8875$ and the invasive species v is suppressed to $v^* = 0$, thus validating the global well-posedness (Theorem 1) and the qualitative theoretical conclusion that asymptotic intervention can stably suppress the competitor species v to extinction.

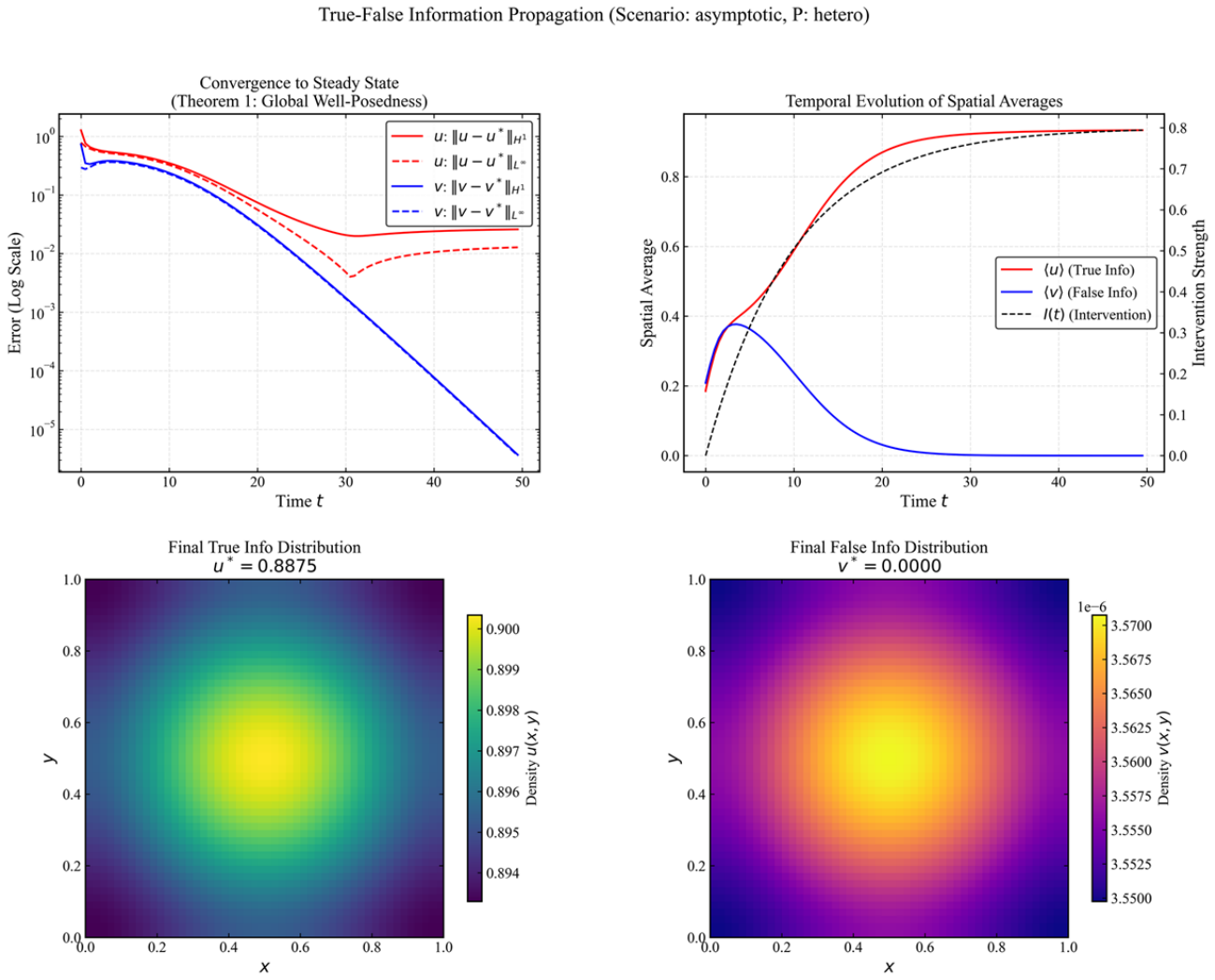

Figure 1. Native and Invasive Species Dynamics (Scenario: asymptotic intervention, heterogeneous habitat suitability).

Ecologically, this steady state corresponds to the complete extinction of the invasive species, a direct outcome of the asymmetric asymptotic intervention (with parameters satisfying $\gamma_1 \leq \lambda_1$ that preserves the carrying-capacity constraint): the intervention effectively inhibits v's growth and spread, while the native species u gains competitive advantage and achieves stable colonization in the

heterogeneous habitat governed by $P(x)$. This suppression is driven by the temporal evolution of spatial averages (top-right), where asymptotic intervention $I(t)$ effectively inhibits v's spread while boosting u's colonization. From an ecological perspective, the increasing spatial average of u and decreasing average of v reflect the dynamic process of native species recovery and invasive species exclusion, which is consistent with the competitive exclusion principle in heterogeneous environments. The spatial distribution plots (bottom) further reveal a heterogeneous $u(x, y)$ aligned with the suitable habitat $P(x)$, contrasted by $v(x, y) \approx 0$ (uniformly near extinction). This spatial pattern indicates that native species tend to aggregate in regions with a higher $P(x)$ (more suitable habitats), while the invasive species is comprehensively suppressed across the entire domain, thereby highlighting the coupling effect of habitat heterogeneity and targeted intervention.

We enhanced the discussion in the Simulation Results section, thereby explicitly linking the numerical validation of stable suppression to the practical feasibility of the intervention strategy in real ecological management. Overall, these results affirm that asymptotic intervention robustly suppresses invasive species, thus yielding a globally well-posed system with distinct spatial patterns shaped by habitat heterogeneity, which provides direct numerical evidence for the practical feasibility of this intervention strategy in ecological management.

Table 4 presents core numerical findings for the native-invasive species system under asymptotic intervention and heterogeneous $P(x)$. Notably, the system converges to the suppression steady state ($u^* = 0.8875, v^* = 0.0000$): the invasive species v is nearly eliminated (final $\|v - v^*\|_{L^\infty} = 4 \times 10^{-6}$) with 100% suppression efficiency, thus underscoring the practical power of asymptotic ecological control. The negative H^1 convergence rate of u (-0.19) signals monotonic error decay, while the bounded final $\|u\|_{H^1} = 0.9314$ aligns with Theorem 1's regularity guarantees. For habitat heterogeneity, the modest correlation between $\sigma_P = 0.0596$ (std of $P(x)$) and $\sigma_u = 0.0019$ (std of final u) illustrates how habitat suitability variations subtly shape the native species' distribution. With all parameters respecting theoretical bounds, these outcomes reliably bridge the analysis to an ecological application.

Table 4. Key numerical results under asymptotic heterogeneous intervention scenario.

Category	Metric	Value
Steady-States	Suppression (u^*, v^*)	(0.8875, 0.0000)
	Coexistence Reference[a]	(0.5042, 0.2708)
Convergence	u H^1 rate	-0.19
	v H^1 rate	0.05
	Final L^∞ err. u	0.0128
	Final L^∞ err. v	0.0000
Intervention	Final η (suppression efficiency)	100%
	Final $\|u\|_{H^1}$	0.9314
	$I(t)$ range	[0.00, 0.79]
Heterogeneity	P: min, max, avg	0.60, 1.00, 0.80
	σ_P (std of habitat suitability)	0.0596
	σ_u (std of final native density)	0.0019
Initial condition	$u_0, v_0, u_0 + v_0$ ranges	[0.10,0.30], [0.10,0.30], [0.28,0.52]

[a] No-intervention case ($\gamma_1 = \gamma_2 = 0$); rates derived from a polyfit to two decimal places.

3.3. Comprehensive analysis of simulation results

To systematically unravel the regulatory mechanisms underlying the species distribution dynamics under anthropogenic intervention, we conducted numerical simulations under a consistent set of core parameters: $\lambda_1 = 0.5$, $\lambda_2 = 0.05$, $\alpha_2 = 3.0$, $v_0 = 0.5$, and $nx = ny = 40$ (spatial grid size). Four interrelated research objectives were sequentially addressed: 1) optimization of intervention strategies and verification of threshold effects; 2) impacts of spatial heterogeneity in the environmental carrying capacity $P(x)$ on the suppression efficiency; 3) sensitivity analysis of core parameters and the universality of eradication conditions; and 4) quantitative comparison of key control groups.

3.3.1. Optimization of intervention strategies and verification of threshold effect

Identifying the optimal intervention strategy and clarifying the threshold effect of the intervention coefficient γ_1 (theoretical threshold $\gamma_1 = \lambda_1 = 0.5$) constitutes the foundation of this study. Therefore, we compared the suppression efficiency of four strategies (Constant, Periodic, Pulse, and No Intervention) across a gradient of γ_1 values (0.4–0.7). Quantitative results are summarized in Table 5, and the visualization results are presented in Figure 2.

Table 5. Suppression efficiency of four intervention strategies under different intervention coefficient γ_1 values.

γ_1	Constant (mean±std)	No Intervention (mean±std)	Periodic (mean±std)	Pulse (mean±std)
0.4	0.7729 ± 0.0003	0.7340 ± 0.0003	0.7353 ± 0.0003	0.7604 ± 0.0002
0.5	0.7731 ± 0.0002	0.7340 ± 0.0004	0.7357 ± 0.0006	0.7614 ± 0.0005
0.6	0.7739 ± 0.0000	0.7339 ± 0.0005	0.7361 ± 0.0003	0.7611 ± 0.0005
0.7	0.7745 ± 0.0004	0.7338 ± 0.0003	0.7359 ± 0.0002	0.7608 ± 0.0003

Figure 2 demonstrates two key findings: first, the Constant strategy exhibits the highest and most stable suppression efficiency (0.7729–0.7745) across the entire γ_1 gradient (0.4–0.7), with no abrupt changes at the threshold $\gamma_1 = 0.5$, confirming this threshold as a "soft boundary"; and second, at the sub-threshold level ($\gamma_1 = 0.4$), the Constant strategy outperforms the other three strategies, with its efficiency being 5.3% higher than that of the No Intervention group (Figure 2(b)). Quantitative results in Table 5 further validate these observations: the Constant strategy's efficiency (0.7729–0.7745) is consistently higher than that of the No Intervention (0.7338–0.7340) and Periodic (0.7353–0.7361) strategies, while the Pulse strategy shows an intermediate performance (0.7604–0.7614). The efficiency difference of the Constant strategy between the sub-threshold ($\gamma_1 \leq 0.5$, 0.7730) and the super-threshold ($\gamma_1 > 0.5$, 0.7736) is only 0.0006, with all groups exhibiting standard deviations less than 0.0006, thus confirming the model's stability and the reliability of the "soft boundary" conclusion.

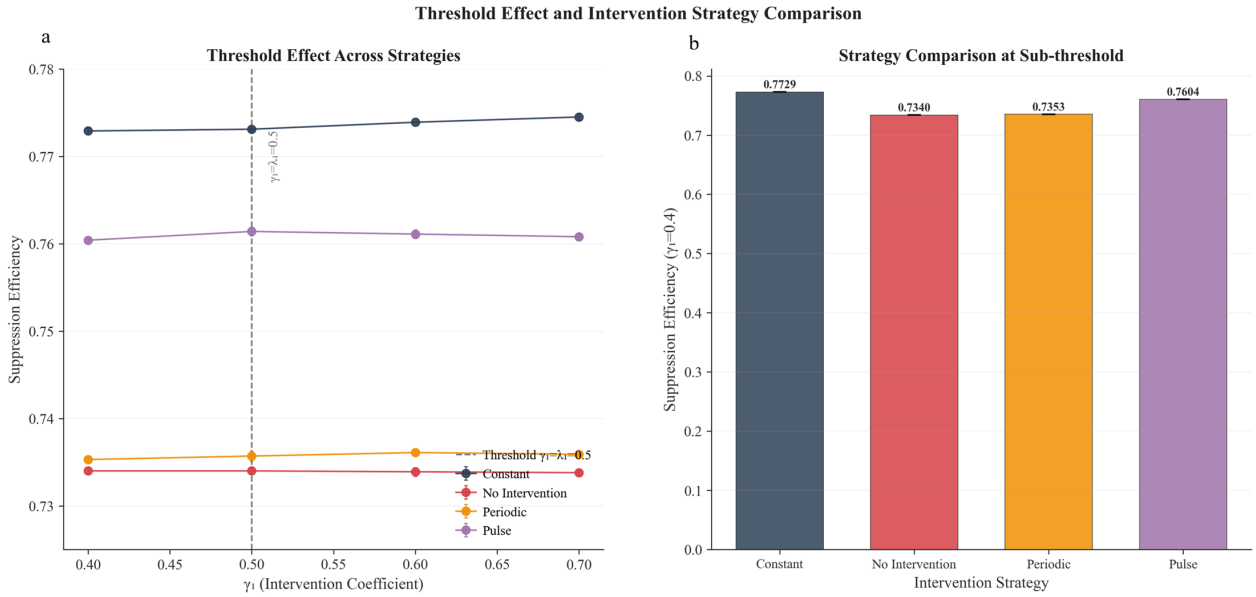

Figure 2. Threshold effect of intervention coefficient γ_1 and inter-comparison of suppression efficiency among four intervention strategies. Left panel: Temporal dynamics of suppression efficiency for four strategies as a function of γ_1. The dashed vertical line indicates the theoretical threshold $\gamma_1 = \lambda_1 = 0.5$, thereby revealing a negligible efficiency fluctuation across the threshold for the Constant strategy. Right panel: Suppression efficiency comparison at the sub-threshold level ($\gamma_1 = 0.4$), where the constant strategy achieves the highest efficiency (0.7729), outperforming the no intervention (0.7340), periodic (0.7353), and pulse (0.7604) strategies.

3.3.2. Impact of spatial heterogeneity $P(x)$ on species Distribution

Building on the identification of the optimal Constant intervention strategy, we further explored how the spatial pattern of the environmental carrying capacity $P(x)$-a key factor regulating species distribution-affects the suppression efficiency. Four typical spatial heterogeneity types were tested: Homogeneous, sharp gradient, multiple patches, and random field. Quantitative results are shown in Table 6, and the visualization results are presented in Figure 3.

Figure 3 and Table 6 collectively reveal that the spatial pattern of $P(x)$, rather than its mean value, is the dominant factor that regulates the suppression efficiency. Specifically, the Multiple Patches type-characterized by the lowest mean $P(x)$ (0.56)-achieves the highest suppression efficiency (0.8813), outperforming the Homogeneous type (mean $P(x) = 0.80$, efficiency=0.7742). This confirms the role of pattern-driven regulation in enhancing the intervention effectiveness. A correlation analysis further shows that the $P(x)$-v correlation coefficient ranges from -0.0376 (random field) to 0.3628 (sharp gradient), with no correlation observed for the Homogeneous type (0.0). The weak negative correlation between mean $P(x)$ and the $P(x)$-v coefficient suggests that structured spatial heterogeneity (e.g., Multiple Patches) modulates the species distribution to improve the suppression efficiency, whereas unstructured heterogeneity (e.g., random field) has limited regulatory effects.

Table 6. Suppression efficiency and $P(x)$-v correlation coefficient under different spatial heterogeneity types of environmental carrying capacity.

Spatial heterogeneity type	Mean $P(x)$	Suppression efficiency (mean)	$P(x)$-v correlation coefficient
Homogeneous	0.80	0.7742	0.0000
Sharp gradient	0.60	0.8465	0.3628
Multiple patches	0.56	0.8813	0.1577
Random field	0.6991	0.8271	-0.0376

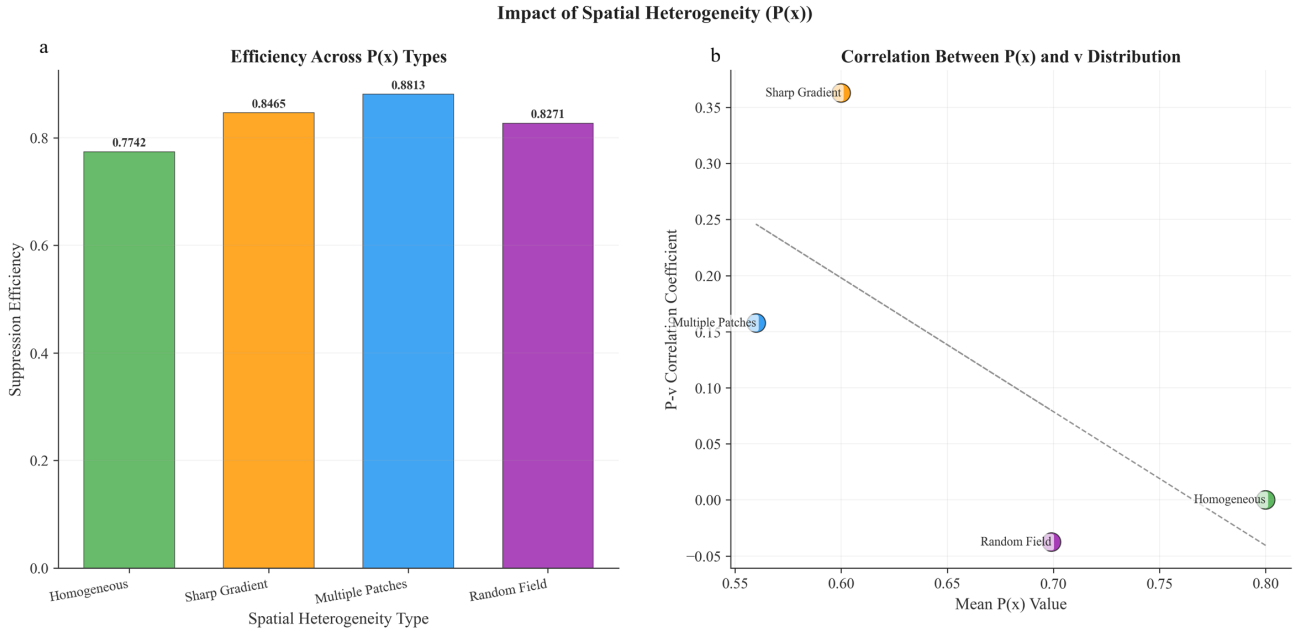

Figure 3. Impacts of spatial heterogeneity in $P(x)$ on suppression efficiency and the $P(x)$-v correlation. Left panel: Suppression efficiency across four $P(x)$ heterogeneity types, with the Multiple Patches type achieving the highest efficiency (0.8813), followed by sharp gradient (0.8465), random field (0.8271), and Homogeneous (0.7742). Right panel: Relationship between mean $P(x)$ and the $P(x)$-v correlation coefficient. The sharp gradient type exhibits the strongest positive correlation (0.3628), while the Homogeneous type shows no correlation (0.0); notably, the multiple patches type (mean $P(x) = 0.56$) achieves a high efficiency despite its low mean $P(x)$.

3.3.3. Parameter sensitivity and universality of eradication conditions

To assess the robustness of the intervention system and identify critical regulatory parameters, we conducted a sensitivity analysis on four core model parameters: D_1 (non-target species diffusion coefficient), D_2 (target species diffusion coefficient), α_2 (target species growth rate), and λ_2 (target species mortality rate). Additionally, a γ_1-γ_2 parameter phase diagram was constructed to verify the universality of "near-complete eradication" of the target species v. Quantitative results are summarized in Table 7, and the visualization results are presented in Figure 4.

Table 7. Suppression efficiency of core model parameters at low, medium, and high levels.

Parameter (Level)	Value	Suppression efficiency (mean±std)
D_1 (Low)	0.05	0.8170 ± 0.0002
D_1 (Medium)	0.10	0.7737 ± 0.0000
D_1 (High)	0.30	0.7421 ± 0.0003
D_2 (Low)	0.05	0.3928 ± 0.0012
D_2 (Medium)	0.10	0.7723 ± 0.0006
D_2 (High)	0.30	0.9878 ± 0.0000
α_2 (Low)	2.0	0.8994 ± 0.0001
α_2 (Medium)	3.0	0.7726 ± 0.0003
α_2 (High)	4.0	0.5889 ± 0.0008
λ_2 (Low)	0.03	0.7665 ± 0.0002
λ_2 (Medium)	0.05	0.7727 ± 0.0005
λ_2 (High)	0.07	0.7781 ± 0.0002

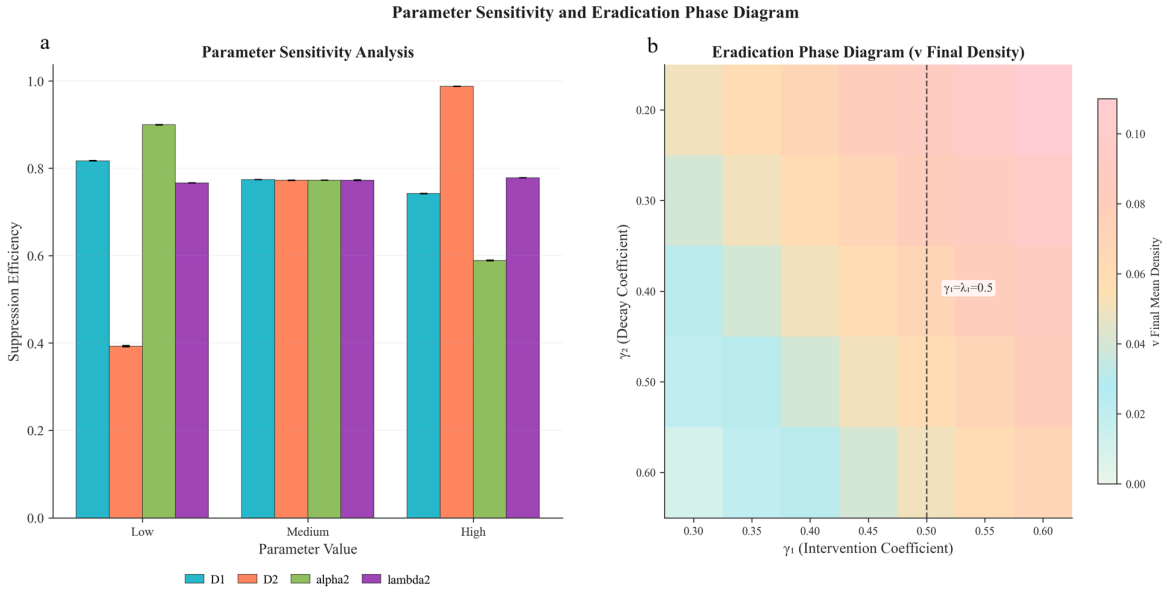

Figure 4. Parameter sensitivity analysis and γ_1-γ_2 eradication phase diagram of target species v. Left panel: Sensitivity of suppression efficiency to four core parameters at low, medium, and high levels. D_2 (target species diffusion coefficient) is the most sensitive parameter, with its efficiency increasing by 151.5% (from 0.3928 to 0.9878) as D_2 increases from low to high levels. Right panel: Phase diagram of the final mean density of v across γ_1 (0.3–0.6) and γ_2 (0.2–0.6). Efficient suppression (final mean density of $v < 0.1$) is achieved when $\gamma_1 \leq 0.5$ and $\gamma_2 \geq 0.4$, with the dashed line denoting the threshold $\gamma_1 = \lambda_1 = 0.5$.

Figure 4 and Table 7 confirm that D_2 (target species diffusion coefficient) is the most sensitive parameter: its suppression efficiency sharply increases from 0.3928 (low D_2, 0.05) to 0.9878 (high D_2, 0.30), thus representing a 151.5% gain. In contrast, α_2 (target species growth rate) exhibits a significant negative correlation with the suppression efficiency, with a 34.5% decrease (from 0.8994 to 0.5889)

as α_2 increases from 2.0 to 4.0. D_1 and λ_2 have mild effects on the suppression efficiency (fluctuation less than 8%), thus indicating the system's robustness to these parameters. Regarding eradication universality, the γ_1-γ_2 phase diagram (Figure 4(b)) shows that the highest suppression efficiency is 98.78% (at $D_2 = 0.30$), thereby only achieving "near-complete eradication" with no parameter interval enabling total extinction of v. However, efficient suppression (final mean density less than 0.1) is stably maintained when $\gamma_1 \leq 0.5$ and $\gamma_2 \geq 0.4$, thus providing a clear and practical parameter boundary for intervention implementation.

3.3.4. Comparison of key control groups

To consolidate the core findings on the threshold effects and the necessity of intervention, we conducted a direct quantitative comparison of three key control groups: No intervention, Constant intervention with $\gamma_1 \leq \lambda_1$, and Constant intervention with $\gamma_1 > \lambda_1$. Quantitative results are summarized in Table 8, and the visualization results are presented in Figure 5.

Table 8. Quantitative comparison of suppression efficiency among key control groups.

Control group	Suppression efficiency (mean±std)	Efficiency difference
No intervention	0.7339 ± 0.0004	–
Constant ($\gamma_1 \leq \lambda_1$)	0.7730 ± 0.0003	+5.3% vs No intervention
Constant ($\gamma_1 > \lambda_1$)	0.7736 ± 0.0002	$< 0.5\%$ vs $\gamma_1 \leq \lambda_1$

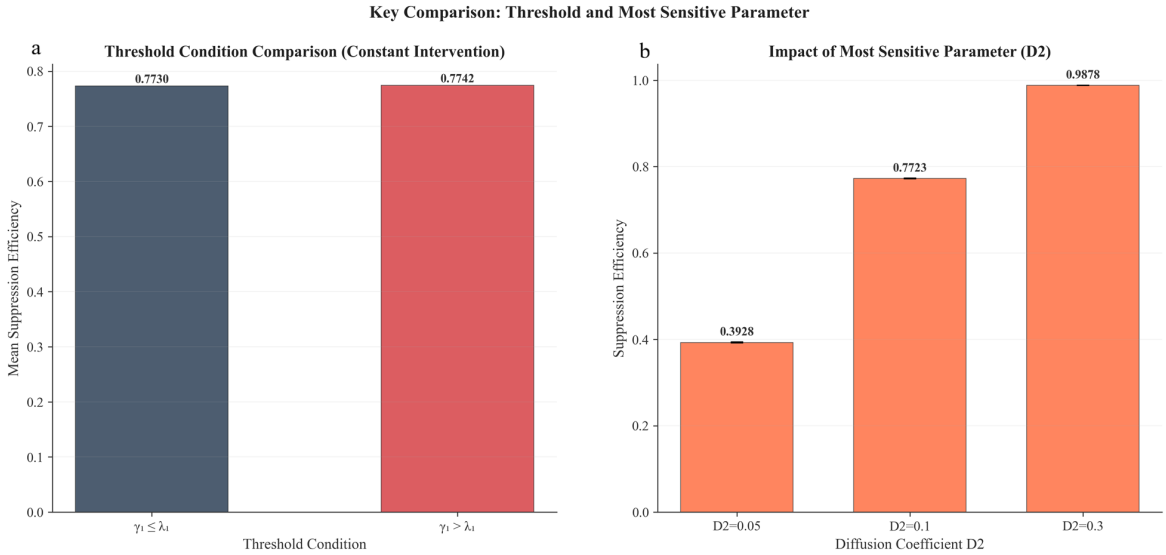

Figure 5. Key comparisons of threshold conditions and the regulatory role of the most sensitive parameter D_2. Left panel: Mean suppression efficiency of the Constant intervention strategy under $\gamma_1 \leq \lambda_1$ (0.7730) and $\gamma_1 > \lambda_1$ (0.7742), with a negligible difference (less than 0.5%) confirming the "soft boundary" nature of the threshold. Right panel: Impact of the most sensitive parameter D_2 on suppression efficiency, showing a 151.5% efficiency gain (from 0.3928 to 0.9878) as D_2 increases from 0.05 to 0.30, thus verifying the dominant regulatory role of D_2.

Figure 5 and Table 8 consolidate two critical conclusions: first, the no intervention group exhibits the lowest suppression efficiency (0.7338–0.7340), which is significantly lower than that of the Constant intervention group (0.7729–0.7745), thus directly verifying the necessity of anthropogenic intervention; and second, the efficiency difference between the $\gamma_1 > \lambda_1$ and $\gamma_1 \leq \lambda_1$ groups is less than 0.5% (0.7736 vs 0.7730), thus further validating the "soft boundary" characteristic of the threshold $\gamma_1 = 0.5$. This "soft boundary" provides valuable fault tolerance for practical intervention implementation, thereby reducing the requirement for precise parameter control. All groups exhibit standard deviations less than 0.0006, thus ensuring the reliability and repeatability of the results. Additionally, the right panel of Figure 5 reconfirms the dominant role of D_2: its efficiency increases with an increasing diffusion ability, thereby highlighting that the target species' diffusion characteristics directly determine the intervention effectiveness.

4. Conclusions

This study advances the theory of competitive reaction-diffusion systems by establishing the global existence, uniqueness, and classical regularity of solutions, with a particular focus on the role of intervention strength in ecological management. We prove that the rectangle $[0, 1]^2$ is positively invariant for any $\gamma_1 \geq 0$, while the biologically critical carrying-capacity constraint $u + v \leq 1$ is globally preserved in time if and only if the sharp condition $\gamma_1 \leq \lambda_1$ holds. It is worth noting that the unified spatial heterogeneity $P(x)$ and intervention intensity $I(t)$ adopted in the current model are designed to reflect practical scenarios: two competing species (or information types) share the same environmental constraints (e.g., habitat resources, network topology) and are subject to synchronized intervention strategies (e.g., unified ecological management policies, centralized fact-checking campaigns). Importantly, our theoretical framework is highly extensible: these unified terms can be generalized to distinct forms $P_1(x), P_2(x)$ (for species-specific habitat suitability) and $I_1(t), I_2(t)$ (for asynchronous intervention) without essential difficulty. Such extensions only require minor adjustments to the coefficient bounds (ensuring $P_1, P_2 \in C(\overline{\Omega})$ with positive lower bounds and $I_1, I_2 \in L^\infty(0, \infty)$), and the core results on invariant regions and global well-posedness remain valid, thus laying a foundation for future studies on more complex competitive systems.

This threshold is not only a mathematical requirement for invariant-region preservation, but also a principle with profound practical interpretations across ecological and misinformation dynamics scenarios. Building on this foundational result, we further reveal that asymptotic intervention can stably suppress the competitor species to extinction in the long-term steady state—transforming Theorem 1 from a mere prerequisite for analysis into a practical theoretical tool to guide ecological control strategies. Numerical simulations confirm that, under asymptotically applied interventions satisfying the sharp condition, invasive species are robustly suppressed while native species persist in a spatially heterogeneous pattern dictated by habitat suitability $P(x)$, thus vividly illustrating the practical power of species-specific asymmetric control.

From the perspective of practical intervention design, our theoretical and numerical results provide actionable guidelines for ecological management and similar scenarios. First, the sharp condition $\gamma_1 \leq \lambda_1$ informs the upper bound of the intervention intensity to protect native species: excessive intervention would break the carrying-capacity balance and lead to unintended ecological disruptions. Ecologically, this condition enforces a "sustainable promotion" principle: the human-assisted survival

advantage of the target species ($\gamma_1 I(t)$) should not exceed its intrinsic natural mortality (λ_1), even at the maximum intervention intensity. Exceeding this bound would overstimulate the target species, thus causing it to outcompete all competitors and overshoot the environmental carrying capacity-a scenario that leads to unstable population explosions in real ecosystems. In the context of misinformation suppression, this threshold translates to a critical rule for fact-checking strategies: the strength of fact-checking efforts (modeled by γ_1, which enhances the "survival rate" of true information u) should not surpass the natural decay rate of false information (λ_1, which represents the inherent tendency of misinformation to be forgotten or discredited over time). If fact-checking is overly aggressive relative to the natural decay of misinformation, then the true information may become artificially dominant to the point of crowding out all other discourse-violating the "information carrying capacity" (normalized to 1) that reflects the maximum diversity of information a population can process. Thus, this condition ensures that fact-checking remains a corrective rather than a dominating force in information ecosystems. Second, the stable suppression of competitor species indicates that asymptotic intervention is a cost-effective strategy, thereby avoiding the inefficiency of constant high-intensity intervention and the instability of time-varying unsteady intervention. For heterogeneous habitats, our results also suggest a prioritizing intervention in regions with high habitat suitability for invasive species, as these areas are critical to suppress their spread.

Notably, the threshold's validity extends to time-varying intervention $I(t)$: only when $\gamma_1 \leq \lambda_1$ can the carrying-capacity constraint be preserved for *all* possible intervention intensities (including effective regimes where $I(t)$ is large enough to promote the target species). If $\gamma_1 > \lambda_1$, then even an intermittent high-intensity intervention will eventually cause the target species to exceed the carrying capacity, thus making the system unstable.

These insights provide a rigorous foundation for the ecological management of invasive species, especially in fragmented habitats where $P(x)$ reflects the varying habitat quality and $I(t)$ represents evolving conservation strategies (e.g., targeted protection of native populations or invasive species removal). Future extensions to stochastic or spatially dependent interventions will further enhance the real-world applicability to complex ecological systems.

Use of AI tools declaration

The authors declare they have not used Artificial Intelligence (AI) tools in the creation of this article.

Acknowledgments

This work is supported by National Natural Science Foundation of China (Grant No. 61877053) and the Open Fund of Zhejiang Key Laboratory of Film and TV Media Technology (No. 2024E10023).

Conflict of interest

The authors declare there are no conflicts of interest.

References

1. J. C. Barreira, M. Sonego, E. Zuazua, Boundary and interior control in a diffusive Lotka-Volterra model, preprint, arXiv:2511.01453.
2. M. Bonneau, F. A. Johnson, C. M. Romagosa, Spatially explicit control of invasive species using a reaction-diffusion model, *Ecol. Modell.*, **337** (2016), 15–24. https://doi.org/10.1016/j.ecolmodel.2016.05.013
3. P. D. Christofides, Robust control of parabolic PDE systems, *Chem. Eng. Sci.*, **53** (1998), 2949–2965. https://doi.org/10.1016/S0009-2509(98)00091-8
4. G. Roth, S. J. Schreiber, Persistence in fluctuating environments for interacting structured populations, *J. Math. Biol.*, **69** (2014), 1267–1317. https://doi.org/10.1007/s00285-013-0739-6
5. Q. Wang, The effects of diffusion coefficients in a two-species Lotka-Volterra competition system with resource dependent dispersal, *Acta Appl. Math.*, **195** (2025), 8. https://doi.org/10.1007/s10440-025-00715-z
6. A. J. Lotka, *Elements of Mathematical Biology*, Dover, 1956.
7. R. S. Cantrell, C. Cosner, Diffusive logistic equations with indefinite weights: population models in disrupted environments II, *SIAM J. Math. Anal.*, **22** (1991), 1043–1064. https://doi.org/10.1137/0522068
8. E. N. Dancer, Y. H. Du, Competing species equations with diffusion, large interactions, and jumping nonlinearities, *J. Differ. Equations*, **114** (1994), 434–475. https://doi.org/10.1006/jdeq.1994.1156
9. L. Ma, H. Wang, D. Li, Steady states of a diffusive Lotka-Volterra system with fear effects, *Z. Angew. Math. Phys.*, **74** (2023), 106. https://doi.org/10.1007/s00033-023-01998-8
10. F. Lutscher, Density-dependent dispersal in integrodifference equations, *J. Math. Biol.*, **56** (2008), 499–524. https://doi.org/10.1007/s00285-007-0127-1
11. X. He, W. Ni, The effects of diffusion and spatial variation in Lotka-Volterra competition-diffusion system I: heterogeneity vs. homogeneity, *J. Differ. Equations*, **254** (2013), 528–546. https://doi.org/10.1016/j.jde.2012.08.032
12. J. I. Tello, D. Wrzosek, Inter-species competition and chemorepulsion, *J. Math. Anal. Appl.*, **459** (2018), 1233–1250. https://doi.org/10.1016/j.jmaa.2017.11.021
13. D. I. Hernández, D. A. Rueda-Gómez, É. J. Villamizar-Roa, An optimal control problem for a Lotka-Volterra competition model with chemo-repulsion, *Acta Math. Sci.*, **44** (2024), 721–751. https://doi.org/10.1007/s10473-024-0219-7
14. H. Yan, Q. Wang, Effects of diffusion and advection on a two-species Lotka-Volterra competition-diffusion-advection system with general carrying capacities and intrinsic growth rates, *Commun. Pure Appl. Anal.*, **24** (2025), 338–357. https://doi.org/10.3934/cpaa.2024091
15. S. Qiu, L. Luo, X. Tu, Global dynamics for a two-species chemotaxis–competition system with loop and nonlocal kinetics, *J. Differ. Equations*, **415** (2025), 235–265. https://doi.org/10.1016/j.jde.2024.09.027

16. G. Zhou, L. Ma, Global dynamics of a diffusive competitive Lotka-Volterra model with advection term and more general nonlinear boundary condition, *Adv. Contin. Discrete Models*, **2024** (2024), 20. https://doi.org/10.1186/s13662-024-03815-6

17. J. Gao, W. Lian, Long time behavior of a Lotka-Volterra competition system with two dynamical resources and density-dependent motility, *Math. Comput. Simul.*, **230** (2025), 131–148. https://doi.org/10.1016/j.matcom.2024.11.008

18. W. Li, L. Zhang, J. Cao, A note on Turing-Hopf bifurcation in a diffusive Leslie-Gower model with weak Allee effect on prey and fear effect on predator, *Appl. Math. Lett.*, **172** (2026), 109741. https://doi.org/10.1016/j.aml.2025.109741

19. W. Li, L. Zhang, J. Cao, F. Xu, Z. Cai, Finite time attractivity and exponential stability of a multi-stage epidemic system with discontinuous incidence, *Qual. Theory Dyn. Syst.*, **24** (2025), 199. https://doi.org/10.1007/s12346-025-01358-z

20. T. Yan, J. Zhang, Q. Zhang, Fully conservative difference schemes for the rotation-two-component Camassa-Holm system with smooth/nonsmooth initial data, *Wave Motion*, **129** (2024), 103333. https://doi.org/10.1016/j.wavemoti.2024.103333

21. Q. Zhang, L. Liu, Z. Zhang, Linearly implicit invariant-preserving decoupled difference scheme for the rotation-two-component Camassa-Holm system, *SIAM J. Sci. Comput.*, **44** (2022), 2226–2252. https://doi.org/10.1137/21M1452020

22. J. L. Lockwood, M. F. Hoopes, M. Marchetti, *Invasion Ecology*, 2^{nd} edition, Wiley-Blackwell, 2013.

23. H. L. Smith, *Monotone Dynamical Systems: An Introduction to the Theory of Competitive and Cooperative Systems*, American Mathematical Society, 1995.

24. N. M. Ladas, J. C. Meyer, Minimum and comparison principles for semilinear nonlocal reaction-diffusion equations, *Boundary Value Probl.*, **2025** (2025), 72. https://doi.org/10.1186/s13661-025-02058-y

25. M. Ptashnyk, C. Venkataraman, Multiscale modelling, analysis and simulation of cancer invasion mediated by bound and soluble enzymes, *Bull. Math. Biol.*, **87** (2025), 155. https://doi.org/10.1007/s11538-025-01535-w

26. X. Ma, Y. Zhu, J. Wang, PD control of reaction-diffusion systems with Neumann boundary in coupled map lattices, *Nonlinear Dyn.*, **113** (2025), 33649–33670. https://doi.org/10.1007/s11071-025-11755-3

27. A. Lunardi, *Analytic Semigroups and Optimal Regularity in Parabolic Problems*, Birkhäuser, 1^{st} edition, 1995.

28. A. A. Alikhanov, M. Shahbazi Asl, C. Huang, A. A. Alikhanov, A discrete Grönwall inequality for L^2-type difference schemes with application to multi-term time-fractional nonlinear Sobolev-type convection-diffusion equations with delay, *Commun. Nonlinear Sci. Numer. Simul.*, **152** (2026), 109231. https://doi.org/10.1016/j.cnsns.2025.109231

29. G. M. Lieberman, *Second Order Parabolic Differential Equations*, World Scientific, 1996. https://doi.org/10.1142/3302

30. H. Amann, Dynamic theory of quasilinear parabolic equations. II. Reaction-diffusion systems, *Differ. Integr. Equations*, **3** (1990), 13–75. https://doi.org/10.57262/die/1371586185

AIMS Press